Contrib Mineral Petrol (2003) 144: 722–738
DOI 10.1007/s00410-002-0425-y

ORIGINAL PAPER

George B. Morgan VI · David London

Trace-element partitioning at conditions far from equilibrium: Ba and Cs distributions between alkali feldspar and undercooled hydrous granitic liquid at 200 MPa

Received: 21 February 2002 / Accepted: 2 October 2002 / Published online: 5 December 2002

Abstract This study examines the effects of increasing supersaturation, attained by single-step liquidus undercooling (ΔT), on the partitioning of barium and cesium between potassic alkali feldspar (Afs) and hydrous granitic liquid at 200 MPa. The investigation is motivated by trace-element distribution patterns in granitic pegmatites which cannot be simulated by fractionation models using "equilibrium" partition coefficients, and thus its purpose is to assess if, how, and why partition coefficients for compatible and incompatible trace elements may vary when crystal growth commences far from the crystal–melt equilibrium boundary. Barium expands the liquidus stability field of potassic feldspar to higher temperatures, such that liquidi for the Ba-rich ($\sim$0.5 wt% BaO) compositions used are $\sim$100 °C higher than for Ba-absent analogues. At low degrees of undercooling ($\Delta T \sim 50$ °C), values of $D_{Ba}^{Afs/m.}$ ($\sim$10–20) fall within the range of previous investigations, as do values of $D_{Cs}^{Afs/m.}$ (≤ 0.10) from experiments at all temperatures. Progressively greater undercooling is manifested in the run products by increasingly skeletal to cuneiform crystal morphologies, increased compositional zonation of Afs, and the development of compositional boundary layers in glass. Whereas the partitioning behavior of Cs (incompatible) is not measurably affected, strong undercooling apparently causes the partitioning of Ba (highly compatible) to deviate from equilibrium behavior. Feldspars produced by strong undercooling ($\Delta T \geq 100$ °C) are heterogeneous, such that $D_{Ba}^{Afs/m.}$ versus $K/K+Na$ varies linearly between the average value at 850 °C and the equilibrium value appropriate to the temperature of growth. Hence, high supersaturation accompanying undercooling produces feldspar compositions by isothermal growth which record a vestige of the liquid line of descent (i.e., an ontogeny within zoned crystals which approximately tracks the feldspar liquidus from high temperature to the final low temperature of actual crystal growth). Such zoning patterns may mimic normal patterns produced by fractionation with decreasing temperature under near-equilibrium (near-liquidus) conditions. Increasing fluorine contents tend to exacerbate the effects of undercooling by inhibiting feldspar nucleation, causing both $K/K+Na$ ratios and compatible trace-element partitioning behavior in feldspar to deviate from equilibrium values. This effect continues until nucleation lag is overcome, whereupon a period of rapid growth from supersaturated liquid follows which is similar to that in F-absent compositions. **Electronic Supplementary Material** to this paper can be obtained by using the Springer LINK server located at http://dx.doi.org/10.1007/s00410-002-0425-y.

Introduction

Large ion lithophile elements (e.g., Sr, Ba, Rb, Cs) figure prominently in modeling magmatic fractionation (e.g., McCarthy and Hasty 1976; Irving 1978; Harris and Inger 1992). Although some disparity exists in absolute values, the partition coefficients for Ba ($D_{Ba}^{Afs/m.}$) and Cs ($D_{Cs}^{Afs/m.}$) between alkali feldspar and granitic liquids are comparatively well known. Examination of experiments (Long 1978; Carron and Lagache 1980; Guo and Green 1989; Icenhower and London 1996) and natural rocks (see Discussion) shows that most of the disparities observed in the partition coefficients, especially for Ba, arise primarily from differences in temperature, pressure, and feldspar composition. Because at least a local approach to crystal–melt equilibrium is

Electronic Supplementary Material to this paper can be obtained by using the Springer LINK server located at http://dx.doi.org/10.1007/s00410-002-0425-y.

G.B. Morgan VI (✉) · D. London
School of Geology and Geophysics, University of Oklahoma, 100 East Boyd Street, SEC 810, Norman, Oklahoma 73019, USA
E-mail: gmorgan@ou.edu
Tel.: +1-405-3252642
Fax: +1-405-3253140

Editorial responsibility: T.L. Grove

fundamental to using partitioning behavior in petrologic modeling, one aspect not previously treated experimentally is the effect of supersaturation promoted by extreme liquidus undercooling on element partitioning. In a previous study of feldspar growth, Fenn (1977) pointed out that supersaturation of melt, usually achieved via some magnitude of liquidus undercooling, is requisite to initiate and sustain crystal growth. Although perhaps not so important for large or deeply emplaced granitic bodies, crystal growth at high degrees of supersaturation is endemic to small, shallowly emplaced granitic dikes and pegmatites. Heat loss from many such bodies is so rapid (e.g., London and Morgan 1998; Webber et al. 1999) that they cool to, or below, their solidi on time scales shorter than the nucleation delays observed in experiments with comparable compositions (Kovalenko and Kovalenko 1984; London 1992; London and Morgan 1998). For example, calculations for the ~2.2-m-thick Little Three pegmatite-aplite dike (Morgan and London 1999) indicate that the outer 20% of the dike reached its solidus in less than three days, and the entire body was below the solidus in about 20 days. Major-element feldspar compositions in the body track primary crystallization along an approximately 400 °C isotherm which advanced from the margins inward through the dike. Hence, consolidation of the body occurred extremely rapidly from grossly undercooled media. In that same study, we also monitored variations in trace- and minor-element (e.g., Mn and F) concentrations in tourmaline and mica to better understand the process of crystallization throughout the dike section. For the phases and trace elements chosen, fractional crystallization models using published near-equilibrium partition coefficients failed to reproduce the trace-element trends across the dike. We noted, however, that considerable uncertainty in identifying the likely fractionation processes may have been introduced because equilibrium crystal–melt partition coefficients may not be applicable to such a strongly undercooled system.

There are two basic concerns for applying "equilibrium" partition coefficients to model crystal growth far from equilibrium. The first is whether supersaturation in an undercooled liquid perturbs the composition–temperature relation for a mineral group or solid-solution series, i.e., are feldspar compositions grown from a given bulk composition at a given temperature independent of the time–temperature path taken to the final state? Although perhaps not important for highly incompatible components, this question is especially germane to highly compatible trace elements for which the $K_d^{Xtal/liq}$ values increase with temperature (e.g., Ba in K-feldspar and, perhaps, Ca in sodic alkali feldspar). Restated, the question is whether the growth of a crystal far from equilibrium (1) retains the equilibrium $K_d(i)$ relationship which applies to the actual conditions of growth, or (2) does the condition of crystal growth far from the crystal–melt equilibrium fundamentally change $K_d(i)$? In either case, a zoned crystal with decreasing trace-element abundance from core to rim would be expected, although the crystal may be homogeneous with respect to major elements. For the first case, the constancy of $K_d(i)$ could be assessed by comparing $K_d(i)$ for crystal rim–melt (or groundmass) pairs to a value of $K_d(i)$ reconstructed from the concentration of component (i) at the crystal core divided by the bulk concentration (i) of the whole rock, assuming that the mineral in question was one of the first phases to crystallize. In the second case, increased lattice strain caused by higher defect density (e.g., Tilley 1987) may lead to higher initial values of $K_d(i)$ (e.g., see Blundy and Wood 1994), but with $K_d(i)$ decreasing and $[i]_{Xtal}$ decreasing more rapidly from core to rim than in the first case. The crystal would then have the appearance of having started to crystallize at higher temperature (in this model, $K_d(i)$ increases with T), but major-element composition may otherwise be homogeneous, or not. Figure 1 helps to illustrate these possibilities in a completely miscible, binary solid solution for which a liquid of composition X is cooled from T_1 to T_2 before crystallization commences. What will the composition of the resultant crystalline phase be upon isothermal crystallization at T_2? Will it be more like homogeneous crystals of composition X, or zoned crystals with compositions spanning the range of Y→Z? To our knowledge, there is no existing theoretical analysis which predicts the resultant composition, although we have noted in many previous experiments with feldspar-bearing systems (e.g., London et al. 1989) that the feldspars so grown are zoned as Y→Z from core to rim (and coexist with metastable liquid, as at Z in Fig. 1).

The second concern for applying equilibrium partition coefficients to undercooled systems deals with the rate of crystal growth in relation to the diffusivity of components through liquid. In highly undercooled and viscous silicate magmas, crystal growth rates may exceed the rates at which incompatible components can diffuse away from the crystal interface, or may be limited by the rate at which compatible components can be supplied to the crystal surface. The diffusion of major components through melt becomes the rate-limiting control on crystal growth, but values of $K_d(i)$ for trace elements can be expected to change with the composition of the boundary layer of melt which develops at the crystal

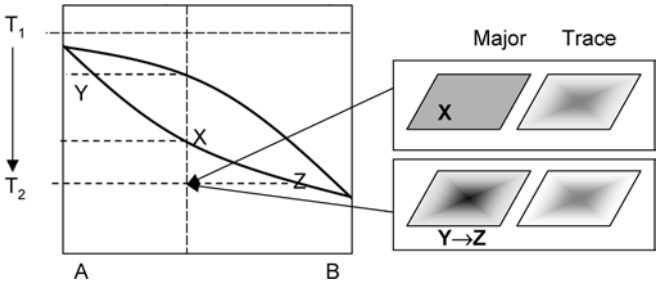

Fig. 1 Schematic representation of potential crystal zoning patterns produced in undercooled liquid of composition X (see text for explanation)

interface. Because the boundary layer may have a composition far from that of the bulk liquid, the actual values of $K_d(i)$, if composition-dependent, will be different from those of the near-equilibrium condition. For example, highly compatible components may be either depleted from the boundary layer or incorporated according to their stoichiometry in bulk liquid, effectively lowering their $K_d(i)$ relative to the bulk system near equilibrium. Conversely, the concentrations of incompatible components may increase above equilibrium values due to concentration in the boundary layer, and perhaps their effective $K_d(i)$ also may increase accompanying rapid growth (e.g., Lindstrom et al. 1979) and/or increased defect densities in crystals. Modeling such scenarios, however, requires knowledge of the boundary layer composition and $K_d(i)$ appropriate to that composition, and hence, knowledge of the rates of crystal growth in relation to component diffusion through melt. These parameters are non-unique, exceedingly variable, and generally intractable. For this reason, the study here is not directly applicable to a natural environment, except by chance that the experiments closely replicate an actual cooling event from a melt of similar composition. What we seek, however, is to learn the nature of the partitioning behavior for a general case of growth far from the crystal–melt equilibrium.

In this study, we examine the effect of supersaturation, achieved by rapid liquidus undercooling and subsequent isothermal growth, on the partitioning of Ba (compatible) and Cs (incompatible) between potassic alkali feldspar and hydrous metaluminous haplogranitic liquid at 200 MPa. In granitic systems, fluorine is known to decrease liquidus and solidus temperatures (Wyllie and Tuttle 1961; Manning 1981), decrease liquid viscosity (Dingwell et al. 1985), and enhance metastable persistence of silicate liquid by suppressing feldspar nucleation upon cooling (London 1987; London et al. 1989). Mineral chemistries and melt inclusion compositions indicate that many shallow granite-pegmatite systems contain F at the weight percent level, or higher, at some point during their evolution (e.g., Morgan and London 1999; London et al. 2001). Therefore, the addition of F not only has relevance to granitic systems, but it introduces an incompatible fluxing component which can be concentrated in a boundary layer and which will strongly influence crystal nucleation (Swanson and Fenn 1992).

Methods

Experimental methods

To provide a reasonable and attainable temperature interval between liquidus and solidus, the bulk composition chosen for study is about 20 wt% richer in the Or component than that of the 200 MPa, H_2O-saturated haplogranite minimum (e.g., Tuttle and Bowen 1958). The compositions of starting materials (other than the Ba- and Cs-feldspar gels which were assumed to be on composition) are listed in Table 1. The principal component of the base mixture is a glass near the 200-MPa H_2O haplogranitic minimum composition synthesized by Corning Lab Services at 1,800 °C and 1 atmosphere. Fragments of coarsely crushed glass were ground in an agate mortar and pestle under ethanol to a mean grain size of ≤ 20 μm. Approximately 20 wt% of similarly ground adularia from Betroka, Madagascar was added to this, plus fired gels of $BaAl_2Si_2O_8$ and $CsAlSi_3O_8$ composition prepared by the method of Hamilton and Henderson (1968). The resultant mixture was then ground under ethanol for about 25 min, dried overnight at 110 °C, and further mixed by tumbling in an oversized jar (volume ~5× that of powder) for 24 h. A split of this base mixture was removed, and ~1 wt% F was added as AgF; this mixture was homogenized by similar grinding, drying, and tumbling. The contents of BaO and Cs_2O in the base composition were targeted at 0.5 wt% each to facilitate analysis by electron microprobe. Anhydrous normalization of electron microprobe analyses (EMPA) on glasses from near-liquidus experiments (850 °C: charges contained $\ll 1$ vol% crystals of near-ideal celsian) demonstrates excellent agreement between the targeted and realized compositions (Table 1).

Deionized and ultra-filtered water (intended to yield ~4–5 wt% H_2O in melt), followed by ~40–50 mg of the powder mixture were loaded into the central, 6–7 mm cavity of 17 mm (L)×3 mm (OD)×0.2 mm (wall) gold capsules. Capsules were frozen with cryogenic spray and then sealed by DC Ar-plasma arc welding. After welding, capsules were compressed to yield charge dimensions of about 5–7 mm (L)×4 mm (W)×1 mm (TH). Capsules were weighed before and after welding, and again after subsequent overnight heating at 110 °C to insure no water loss during welding nor any subsequent leakage.

Experiments were run in subhorizontal Nimonic-105 cold-seal reaction vessels. Capsules were pressurized cold to 1,920–1,960 MPa; pressure was allowed to increase up to 200 MPa during

Table 1 Starting components (values in parentheses are 1-σ standard deviations; *n.d.* not determined)

	Corning glass[a] $n=41$	Betroka Adularia[a] $n=166$	BCs2 target[b]	BCs2-3 anhydrous[c] $n=15$	BCs2F target[b]	BCs2F-2 anhydrous[c] $n=15$
SiO_2	77.63 (0.59)	64.05 (0.04)	74.06	74.48 (0.34)	73.24	73.88 (0.39)
Al_2O_3	13.03 (0.16)	18.67 (0.02)	14.40	14.20 (0.16)	14.24	14.16 (0.14)
CaO	0.01 (0.01)	0.15 (0.00)	n.d.	0.04 (0.02)	n.d.	0.04 (0.02)
Na_2O	4.61 (0.11)	0.71 (0.11)	3.73	3.52 (0.10)	3.69	3.47 (0.12)
K_2O	4.79 (0.09)	15.41 (0.02)	6.70	6.73 (0.13)	6.62	6.77 (0.15)
BaO	n.d.	0.65 (0.01)	0.62	0.57 (0.01)	0.61	0.60 (0.02)
Cs_2O	n.d.	n.d.	0.49	0.46 (0.02)	0.48	0.44 (0.02)
F	n.d.	n.d.	n.d.	0.00 (0.01)	1.12	1.05 (0.07)
O=F	–	–	–	–0.00	–	–0.41
Total	100.07 (0.63)	99.64 (0.12)	100.00	100.00 (0.41)	100.00	100.00 (0.56)

[a]From EMPA
[b]Theoretical (calculated from weights of added components)
[c]From EMPA of experimental product ($\ll 1\%$ crystals) with result normalized to anhydrous composition

the initial heating step, and remained isobaric thereafter. The pressure medium was water with a trace of Immunol added as a rust inhibitor. Pressure was monitored with a factory-calibrated, Heise bourdon-tube gauge with an estimated uncertainty of ≤ 10 MPa, and pressure fluctuations were less than 5 MPa over the course of the experiments. Temperature was monitored with an internal K-type thermocouple (tip approx. even with the capsule center) with an estimated uncertainty ≤ 5 °C. All experiments, with the exception of those with a final run temperature of 850 °C (which were isothermal throughout the duration of the run), were conducted as reverse-direction runs: the first heating (preconditioning) step at 850 °C for 48 h homogenized components in liquid. The temperature was subsequently decreased in a single, isobaric step to the final run conditions. Experiments were quenched isobarically to T ≤ 200 °C using a jet of compressed air and water (10–30 °C/s). Following quench, capsules were weighed to check for potential leakage; any capsules showing significant weight change after run were discarded. Capsules were subsequently punctured to check for the effluence of free water, then heated in a drying oven at 110 °C for 1–3 h and re-weighed to check for loss of free water.

Experiments were conducted in 50 °C increments over the temperature ranges of 850–600 °C for the F-absent system, and 850–550 °C for the F-bearing system, yielding conditions from the stable field of crystals + liquid down to ~90 °C below the apparent solidus of each system.

Analytical methods

Representative fragments of each charge were embedded in low-viscosity ("Spurr") epoxy. Care was taken to mount fragments both parallel (i.e., plan section) and perpendicular (i.e., cross section) to the largest face of the flattened charges, to ensure that a complete and representative sampling of crystals could be observed if heterogeneous nucleation and/or sequential growth occurred inwards from the charge margins. Samples were ground wet to near the center of plan-section fragments using Al_2O_3-impregnated lapping films with grits sizes from 30 to 3 μm, and then polished to a final grit size of 0.25 μm using diamond suspended in water. Petrographic study was accomplished by transmitted and reflected light microscopy, and by backscattered electron imaging (BSEI) coupled with energy-dispersive X-ray analysis (EDXA) on an electron microprobe using 20-kV acceleration and a 5-nA beam current at the sample. Although BSEI was performed mostly prior to quantitative analysis, care was taken to irradiate the sample neither for extended periods nor at high magnification (rasters were > 100×100 μm) prior to analyzing glass in order to prevent the potential migration of alkalis under the beam.

Glasses and crystals were analyzed by electron microprobe at the University of Oklahoma on a Cameca SX50 equipped with five wavelength dispersive spectrometers. Natural and synthetic crystalline materials were used as the primary standards, and data reduction employed the PAP procedure (Pouchou and Pichoir 1985). In order to minimize alkali migration and attendant changes to EMPA results, glasses were analyzed using two-beam conditions as outlined by Morgan and London (1996). An initial 20-kV, 2-nA beam with 20-μm spot was used for Na, Al, Si, K, and Ca (Na and Al were analyzed first and concurrently): counting times were 30 s. A subsequent 20-kV, 20-nA beam with 20-μm spot was used for Ba, Cs, and F. Crystals were analyzed using a 20-kV, 15-nA beam with 2-μm spot size: counting times for Na, Al, Si, K, and Ca were 15 s. Barium was analyzed with a PET diffraction device, using barite as the primary standard: counting times were 45 and 90 s on glass and crystals, respectively, yielding calculated respective minimum detection limits of 0.035 and 0.030 wt% BaO at 3-σ above mean background. Barian adularia and NBS/NIST glass K309 were analyzed as secondary standards for Ba: the results indicated excellent reproducibility of the methods for both low (adularia: 0.32 wt%) and moderate–high (K309: 15.00 wt%) BaO contents in silicate matrices. Cesium also was analyzed using a standard PET device with pollucite (nominally $Cs_2Al_2Si_4O_{12}$) as the standard: the counting times were 45 and 90 s for glass and crystals, respectively, yielding calculated 3-σ minimum detection limits of 0.04 and ~0.03 wt% Cs_2O. Fluorine in glass was analyzed using a W-Si multilayer device (2d = 62.5Å) and synthetic F-phlogopite as the standard: the counting time was 45 s, yielding a calculated minimum detection limit (m.d.l.) of 0.10 wt% F. An experimentally vitrified, hydrous metaluminous rhyolite with ~1.1 wt% F from Spoor Mountain, Utah (SM35: Christiensen et al. 1984; vitrified and furnished by J.D. Webster, U.S. Museum of Natural History: see Morgan and London 1996 for details) was used as a secondary standard for F analysis.

Partition coefficients, $K_d(i)^{Afs/m.}$ (hereafter abbreviated as $D_i^{Afs/m.}$), were calculated directly as $(wt\%\ element)_{crystal}/(wt\%\ element)_{glass}$. In some cases, the concentration of one component in a phase fell below the m.d.l. by EMPA. In such cases the partition coefficient was calculated using the detection limit as the constraining value, and is reported as "> X" where the concentration in glass is below the m.d.l., and "< X" where concentration in crystal is below the m.d.l.

Results

Run products

The experimental results are briefly summarized in Table 2. More information including electron microprobe analyses of the run products is summarized in Appendix 1 (this Electronic Supplementary Material can be obtained by using the Springer LINK server located at http://dx.doi.org/10.1007/s00410-002-0425-y).

Phase relations and textures

The only crystalline products observed in F-absent experiments from 850 °C were traces (≤ 1–2 vol%) of a celsian (Ba-rich) feldspar. This phase also was present in experiments cooled to lower temperature and is presumed to have formed during the initial homogenization step at 850 °C. Experiments at 850 °C with ≤ 4 wt% added H_2O also contained traces (1–3 vol%) of rounded, relict grains of the starting Betroka adularia (verified by EMPA); this phase occurred as inclusions in later feldspar growth (serving as nucleation centers), and also persisted in lower-temperature experiments with comparable added H_2O contents. Relict adularia was not present in charges with > 4.5 wt% added H_2O. A true, K-dominant (but still Ba-rich) alkali feldspar was produced in F-absent experiments at T ≤ 800 °C, and its abundance increased with decreasing T. Quartz was produced only in experiments at T = 600 °C.

Fluorine-bearing experiments with 5 wt% added H_2O were entirely vitric at T≥750 °C, and contained about 2 vol% alkali feldspar at 700 °C. Crystallization at T≥750 °C was observed only in F-bearing experiments which contained < 4 wt% added H_2O. Among those, experiment BC2F-3 (800 °C) was the only such charge which contained traces (< < 1 vol%) of a celsian-rich feldspar, which we also interpret to have formed at 850 °C. That experiment and #BC2F-4 (750 °C) also contained < 1–2 vol% of a Ba-rich but K-dominant alkali feldspar. Relict adularia was not observed in any F-bearing charge. In all experiments, the abundance of

Table 2 Experimental results

Number	T (°C)	Time (days)	H_2O (wt%)[a]	Assemblage[b]	$D_{Ba}^{Afs/m.}$	$D_{Cs}^{Afs/m.}$
F-absent						
BC2-3	850	2	4.98	Cel(< 1) + gl	59.5 ± 21.3[c]	< 0.07
BC2-8	800	5	4.77	Cel(< 1) + Afs(2) + gl	14.9 ± 0.4	< 0.07
BC2-4	800	14	3.96	Cel(< 1) + Afs(15) + rOr(tr) + gl	25.0 ± 1.1	< 0.07
BC2-13	800	14	4.89	Cel(< 1) + Afs(5) + gl	18.9 ± 0.7	0.07 ± 0.06
BC2-9	750	5	4.94	Cel(< 1) + Afs(10–15) + gl	22.2 ± 3.8	0.08 ± 0.06
BC2-5	750	14	4.00	Cel(1) + Afs(30) + rOr(tr) + gl	55.0 ± 15.2	0.07 ± 0.05
BC2-14	750	14	4.91	Cel(1) + Afs(15–20) + gl	32.4 ± 6.9	0.06 ± 0.04
BC2-6	700	5	4.03	Cel(< 1) + Afs(30–35) + rOr(tr) + gl	> 54.0 ± 21.0	0.09 ± 0.09
BC2-10	700	5	4.73	Cel(< 1) + Afs(25) + gl	60.2 ± 13.1	0.07 ± 0.04
BC2-2	700	14	4.66	Cel(< 1) + Afs(35–40) + gl	> 32.6 ± 14.9	0.06 ± 0.03
BC2-11	650	5	4.97	Cel(< 1) + Afs(35) + gl + H_2O	> 53.7 ± 17.8	0.06 ± 0.05
BC2-15	650	14	5.03	Cel(< 1) + Afs(40) + gl + H_2O	> 39.4 ± 26.4	0.08 ± 0.05
BC2-7	600	5	3.86	Cel(< 1) + Afs(65) + rOr(2) + gl ± H_2O	> 44.6 ± 13.3	0.10 ± 0.06
BC2-12	600	5	4.94	Cel(< 1) + Afs(45) + Qtz(tr) + gl ± H_2O	37.7 ± 8.5	0.05 ± 0.03
BC2-1	600	14	4.97	Cel(1) + Afs(70) + Qtz(5) + Nafs(tr) + gl + H_2O	> 40.3 ± 15.9	0.03 ± 0.03
1 wt% F						
BC2F-2	850	2	5.00	gl		
BC2F-8	800	5	4.97	gl		
BC2F-3	800	14	3.86	Cel(< 1) + Afs(< 1) + gl	29.0 ± 2.0[c], 14.0 ± 1.3	< 0.07[c], 0.07 ± 0.10
BC2F-9	800	14	4.92	gl		
BC2F-4	750	5	3.99	Afs(2) + gl	10.8 ± 1.1	< 0.07
BC2F-10	750	14	5.03	gl		
BC2F-5	700	5	3.86	Afs(≤ 5) + gl	7.3 ± 1.4	< 0.07
BC2F-11	700	14	4.97	Afs(2–5) + gl	10.3 ± 1.8	0.09 ± 0.06
BC2F-12	650	14	4.98	Afs(10–15) + gl + H_2O	32.3 ± 4.0	0.09 ± 0.03
BC2F-6	600	5	4.01	Afs(10) + gl ± H_2O	5.1 ± 1.8	0.08 ± 0.06
BC2F-1	600	14	4.94	Afs(40–50) + gl + H_2O	20.5 ± 3.5	0.04 ± 0.03
BC2F-7	550	5	3.98	Afs(15) + Qtz(tr) + gl ± H_2O	3.2 ± 1.3	0.07 ± 0.06
BC2F-13	550	14	5.02	Afs(25–30) + Nafs(tr) + Qtz(10–15)gl + H_2O	47.9 ± 18.3	0.06 ± 0.06

[a] H_2O added to charge
[b] Afs, K-dominant alkali feldspar; Cel, Ba-dominant feldspar; gl, glass; H_2O, free water on quench; Nafs, sodium-dominant feldspar; Qtz, quartz; rOr, relict adularia; values in parentheses are approximate volume percentages
[c] Values are for celsian-dominant feldspars

alkali feldspar increased with decreasing temperature; quartz and sodic feldspar were observed only in experiments run at 550 °C. Consistent with the findings of Manning (1981), the addition of 1 wt% F appears to have suppressed crystallization by at least 40–50 °C relative to the F-absent composition. The absence of crystals in F-added runs with 5 wt% added water at 750 °C could be construed to yield a liquidus depression of ~100 °C relative to the fluorine-absent composition (at comparable added H_2O), but we believe that this is a kinetic effect stemming from the inhibition of nucleation in the F-bearing system. For example, the percentage of crystallization in F-added experiments run for 5 days is generally less than half that of F-absent charges run at 100 °C lower temperatures and comparable duration (e.g., compare runs BC2-11 and BC2F-7 in Appendix 1), whereas at 14-day duration the percentage of crystallization is more similar (e.g., runs BC2-15 and BC2F-13). These results, and the nucleation behavior observed in the F-bearing experiments (see below) echo observations from previous studies (e.g., London et al. 1989) that increasing water contents tend to promote metastable persistence of F-bearing silicate liquids.

The most striking visual aspect of the crystalline products in these experiments is the development of skeletal crystal morphologies and radial growth habit with decreasing temperature (Fig. 2). Alkali feldspar grown from the F-absent composition at 800 °C mostly forms thin, euhedral laths; at 750 °C crystals become subhedral to slightly skeletal, and at T ≤ 650 °C morphologies become decidedly cuneiform. Relations are similar for the F-bearing composition but comparable morphologies are produced at T~50–100 °C lower. With the development of skeletal crystal forms comes a coincident growth in radial clusters, which often nucleate on the high-temperature celsian-rich phase (Fig. 2c, d) or on relict adularia. Backscattered electron imaging of charge cross sections and optical inspection of the entire run products suggest that nucleation occurred internally within the F-absent experiments (Fig. 3a, b), whereas the F-bearing experiments show a marked tendency toward nucleation at the margins of the glass charges (Fig. 3c, d). Sidewall-dominated nucleation in the F-added composition indicates a greater degree of liquid metastability, such that nucleation is stimulated primarily by surface catalysis.

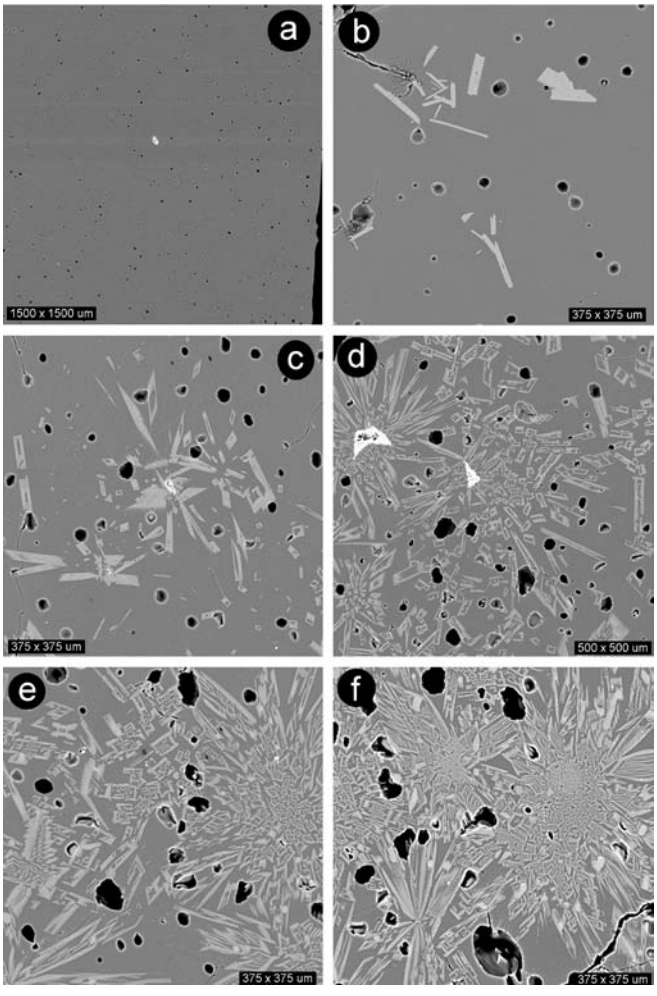

Fig. 2a–f Backscattered electron images from F-absent experiments showing the progressive development of skeletal to cuneiform morphologies with decreasing temperature. **a** 850 °C (BC2-3), **b** 800 °C (BC2-8), **c** 750 °C (BC2-9), **d** 700 °C (BC2-10), **e** 650 °C (BC2-11), **f** 600 °C (BC2-12). All experiments were of 5-day duration, except **a** which was a 2-day control at 850 °C

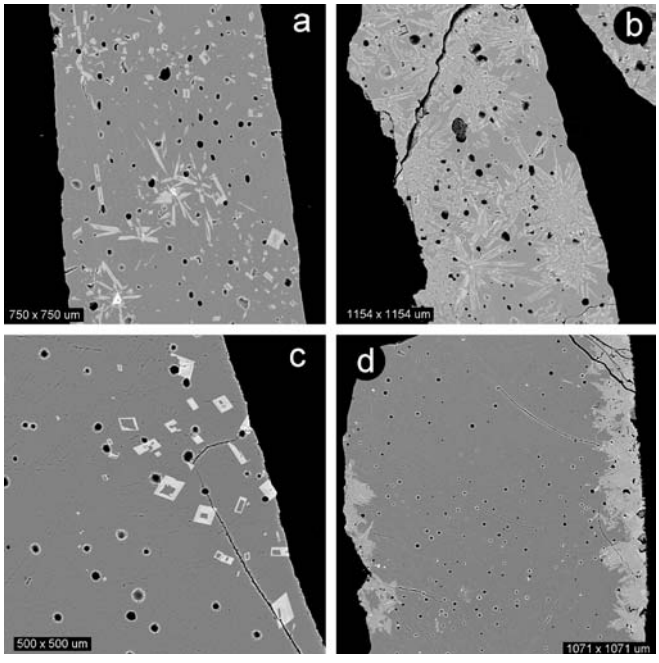

Fig. 3a–d Backscattered electron images of charge cross sections showing internal nucleation in F-absent experiments (**a** BC2-9, 750 °C, **b** BC2-11, 650 °C) versus sidewall-dominated nucleation in F-added experiments (**c** BC2F-4, 750 °C, **d** BC2-7, 550 °C)

Feldspar compositions

Feldspar compositions are plotted in terms of molar Ab–Cel–Or components in Fig. 4. Feldspars produced at 850 °C in the F-absent system have very Ba-rich cores ($Cel_{80–90}$), and Ba-poorer rims ($Cel_{40–60}$), with the trend of compositions crossing the Ab_{10} isopleth at a shallow angle (Fig. 4a). Feldspars produced at 800–700 °C are fairly uniform in composition, but with decreasing temperature they show increasing heterogeneity due to zoning in Ba. Weak zonation is manifested as well-defined, hourglass-shaped sector zoning at T down to 750 °C; at T ≤ 700 °C zoning becomes more irregular as morphologies become more skeletal (Fig. 5). Zoning of skeletal to cuneiform crystals at 600 °C becomes patchy and includes the development of sodic domains intergrown with potassic but still barium-rich (1.4–1.9 wt% BaO) alkali feldspar (Fig. 5c). Overall, the average trend of compositions for feldspars produced below about 700 °C bends off of the trend from higher temperature, towards slightly more sodic compositions (Fig. 4a).

Relations are similar for feldspars in the F-bearing composition but, as a general rule, crystals are more homogeneous down to T = 600 °C (Fig. 4b). Feldspars in short-duration experiments at 550 °C are fairly homogeneous and follow a trend of increasingly potassic compositions established from higher T, but those produced in long-duration experiments show much more varied and more sodic compositions. The reason for increasingly potassic feldspar compositions toward lower temperatures is not exactly clear but may result from a controlling influence of F on melt composition and/or a controlling influence of Ba on feldspar composition. Manning (1981) noted that increasing F content drives the minimum melt composition towards the albite apex in the haplogranite system. Icenhower and London (1996) noted that Ba is more compatible in potassic rather than in sodic alkali feldspars. Liquids in the short-duration experiment at 550 °C are weakly fractionated, containing around 1.4 wt% F (up from ~1 wt% in starting liquid) and molecular K/K + Na = 0.45 (Appendix 1). Even though liquids in the long-duration experiment at 550 °C are much more strongly fractionated, containing ~3.5 wt% F and K/K + Na = 0.30, K-dominant feldspars tend back toward more sodic compositions. Either high barium concentrations are driving K/Na to higher values in feldspar at low percentages of crystallization, or else progressive crystallization (feldspar increasing from about 10 to

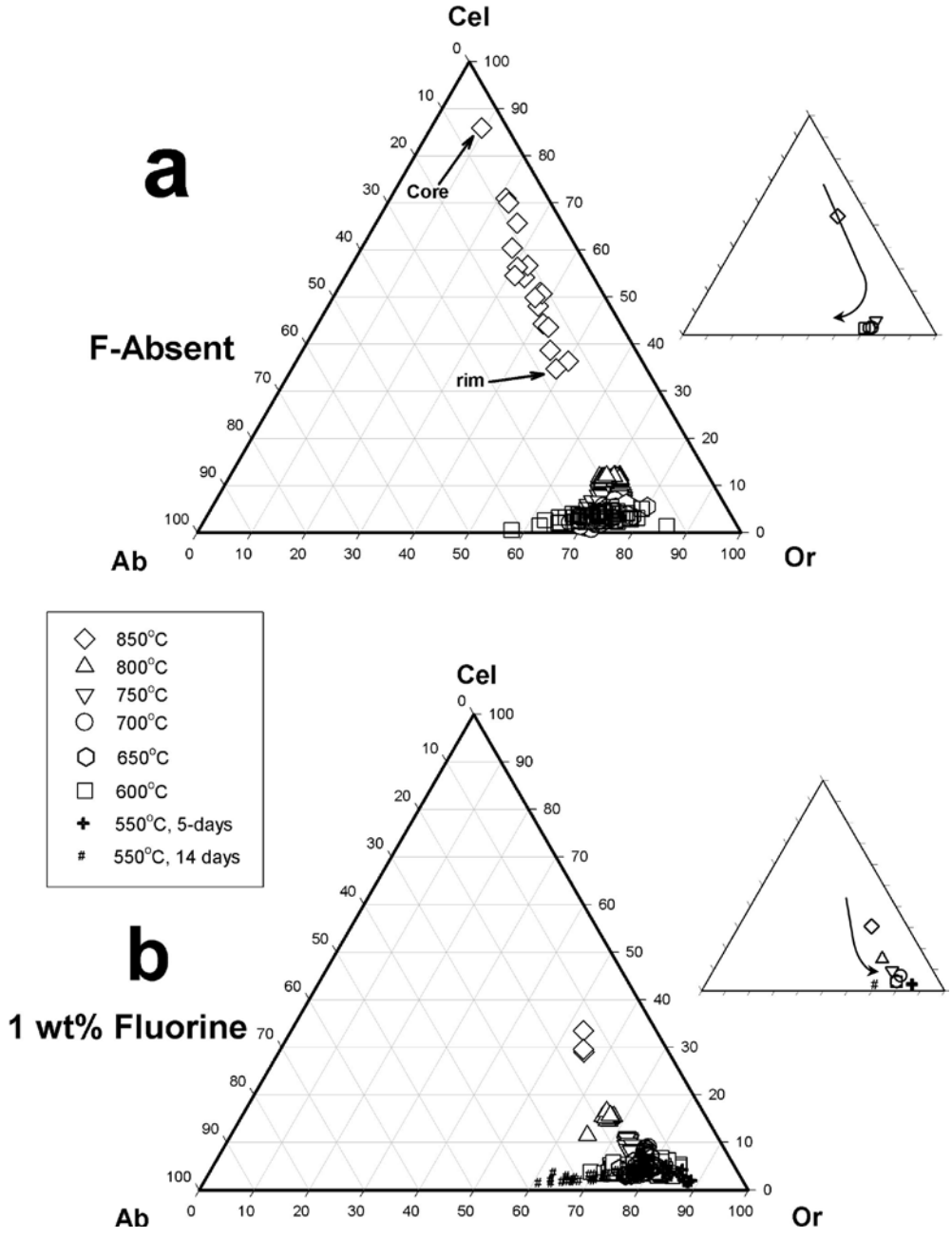

Fig. 4a, b Feldspar compositions plotted as molecular Ab–Cel–Or components. **a** F-absent experiments, **b** 1 wt% F-added experiments. The *larger plots* show all point analyses. *Small plots* show the averages of compositions at each temperature, and the *arrows* indicate trends in composition with decreasing temperature (see text)

30 vol%) has driven the system to become sufficiently oversaturated in the Na component to yield both more sodic but K-dominant feldspar together with a distinctly sodic (albite-rich) phase.

BaO relations between feldspar and glass

The average concentrations of BaO in potassic alkali feldspars (including celsian) and glass as a function of experimental temperature are presented in Fig. 6. The feldspars show a consistent, curved trend of increasing BaO with increasing temperature which corresponds to the curvature of the solidus surface (Fig. 6a). The glasses show a more varied relation that is governed by the percentage of crystallization, which is a function of both temperature and experimental duration, especially for the F-bearing system. A striking observation from Fig. 6 is that at a given experimental temperature, the average BaO content of feldspar is nearly constant regardless of the BaO concentration in glass.

A more direct examination of the relation between BaO contents in crystals and glass is presented in Fig. 7. The F-absent system demonstrates an effectively linear relation over a range of BaO contents from the minimum detection limit up to at least 0.4 wt% BaO in glass, suggesting Henrian behavior throughout this range of composition. The apparent deviation from a Henrian trend at higher BaO in glass likely results from changes in feldspar crystal chemistry, as K-feldspar becomes the

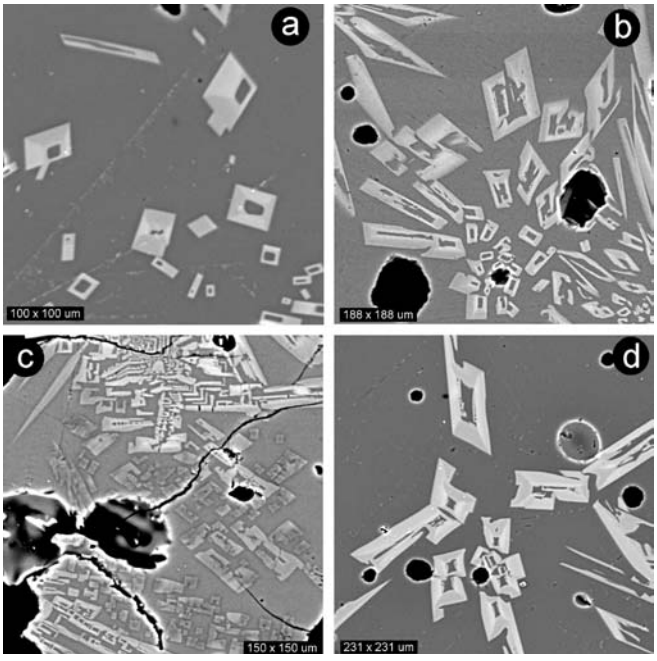

Fig. 5a–d Backscattered electron images showing zoning in alkali feldspar. **a** Hourglass-shaped sector zoning produced at 750 °C in the F-absent system (#BC2-9). **b** Random to sector zoning in skeletal crystals produced at 700 °C in the F-absent system (#BC2-2). **c** Patchy zoning of Ba in potassic phase (*light–medium shading*) and the production of sodic feldspar (*dark shading*) at 600 °C in the F-absent system (#BC2-1). **d** Sector zoning produced at 700 °C in the F-bearing system (#BC2F-5)

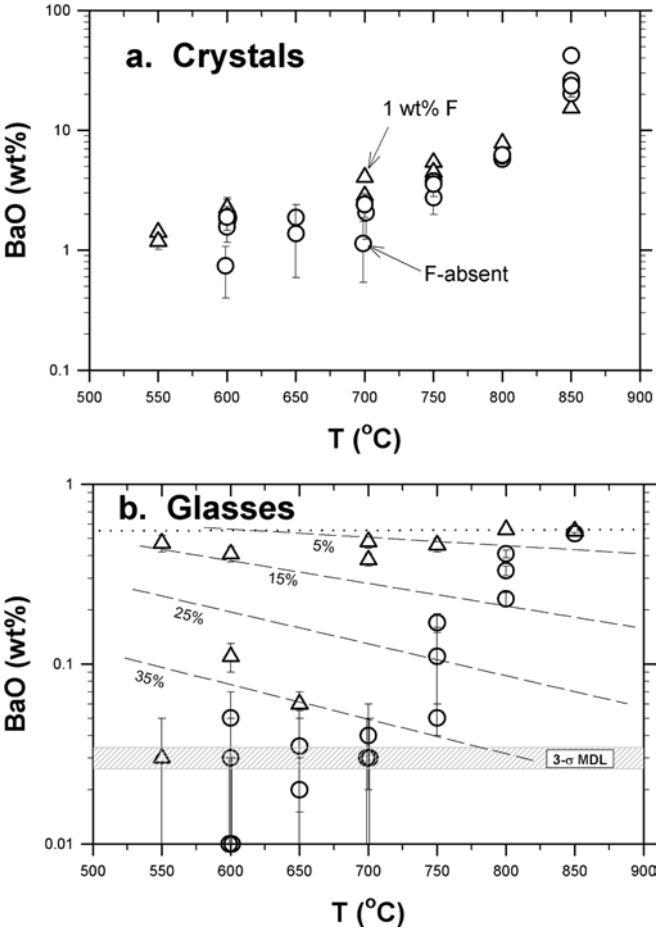

Fig. 6 BaO versus temperature for crystals (**a**) and glasses (**b**). *Error bars* represent 1-σ standard deviations of the microprobe data. The *field* labeled *3-σ m.d.l.* in **b** represents the calculated range of minimum detection limit by EMPA, and the *dashed lines* are contours which indicate approximate percentages of crystals in the experiments

minor component in the high-temperature (850 °C) celsian-dominant phase. Relations are more uncertain in the F-added system. Experiments at T≥700 °C describe a weakly correlated linear trend with very large slope. Short-duration (5-day) experiments at lower temperature are consistent with this trend, but longer duration experiments define a cluster of points more consistent with the results in the F-absent system at similar temperatures. The deviation of the relations for the long-duration, lower-temperature experiments from those at higher temperatures is directly related to the degree of crystallization in the charges. Hence, this argues that kinetic effects (inhibition of crystal growth) hinder the attainment of equilibrium in the F-added system.

H_2O contents of liquid

Although experiments were loaded with 4–5 wt% added water, differences of EMPA totals from 100% indicate higher water contents in glass, even for experiments showing little or no crystallization. Using the current analytical methods (e.g., Morgan and London 1996), we have been successful in replicating the H_2O contents of albite-water glasses containing 2–10% H_2O (Silver and Stolper 1989) to within 6% relative of their concentrations known from conditions of synthesis and FTIR calibration. Therefore, we assume that the water in excess of that loaded in the current experiments is due to adsorption on the starting powders (normally 1–2 wt% in our laboratory). Experiments showing less than ~20 vol% crystallization produced no free water on quench (either by effluence on puncture of the capsule, or subsequent weight change after heating), but H_2O by EMPA difference suggests these charges must have been very near H_2O saturation. Differences in apparent liquidus temperatures between F-added charges with ≤ 4 wt% added H_2O (crystals at 750–850 °C) and those with ~5 wt% added H_2O suggest that charges with the lower H_2O contents were undersaturated at the preconditioning step. Experiments showing more than ~20 vol% crystals have free water on quench, and thus were vapor-saturated at final run conditions.

Boundary layers in glass

The compositions of F-absent glasses (and some F-added glasses) adjacent to large crystal clusters from experiments at T ≤ 750 °C are different from glasses in melt

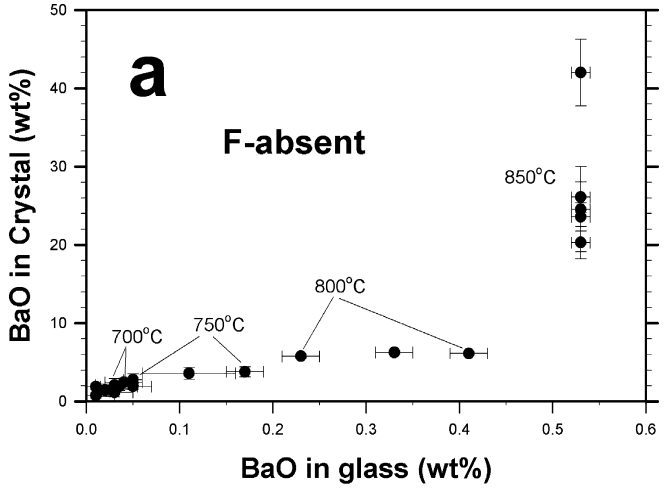

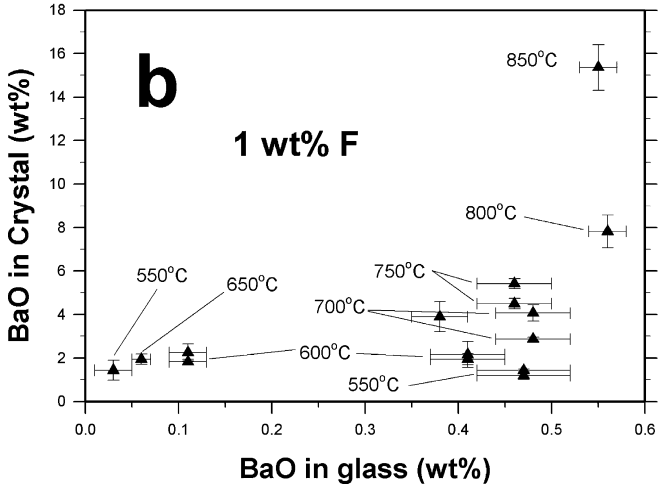

Fig. 7 Average BaO (wt%) in crystals versus glass for F-absent (**a**) and 1 wt% F (**b**) experiments. *Error bars* represent 1-σ standard deviations from the average of microprobe results

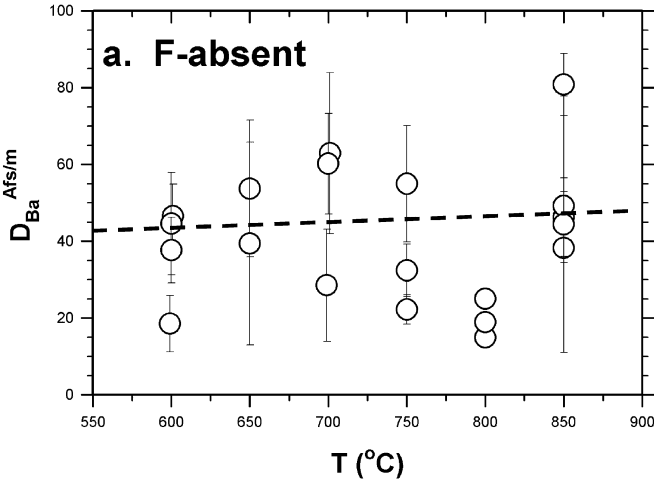

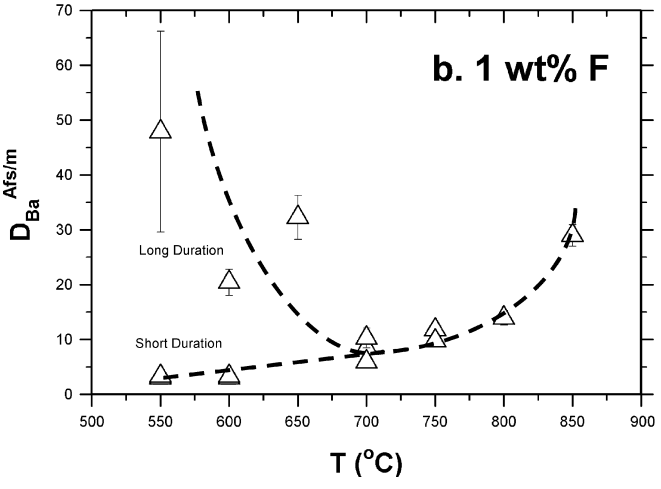

Fig. 8 $D_{Ba}^{Afs/m.}$ versus temperature for F-absent (**a**) and 1 wt% F-added experiments (**b**). *Error bars* represent 1-σ standard deviations from the microprobe data. *Dashed lines* represent inferred trends (see text)

pools removed from crystallization centers. The principal differences are in higher SiO_2, Na_2O, and Cs_2O, and lower Al_2O_3, BaO, and K_2O adjacent to the crystals. The observed variations record the preservation of compositional boundary layers in liquid. In cases where such compositional variations were observed in glass, partition coefficients were calculated using the composition of the glass adjacent to the crystals. We note that compositional gradients in glass are likely to be sharper than can be resolved with the 20-μm spot used for EMPA. Therefore, the partition coefficients for Ba are likely to be underestimated whereas those for Cs will be overestimated.

Cs partitioning

Cesium was found to be strongly incompatible in alkali feldspar at all temperatures. Cesium excluded during crystal growth showed elevated concentrations in the preserved boundary layers in glass. The partition coefficients, $D_{Cs}Afs^{/m.}$, were ≤ 0.10 at all temperatures.

Ba partitioning

Effective partition coefficients, averaged by experiment, are plotted as a function of temperature in Fig. 8. In the F-absent system (Fig. 8a), crystal zoning and boundary layers in liquid (compositional gradients in glass) lend considerable variation in values for temperatures below 750 °C (e.g., values plotted in Fig. 8a are averages for each experiment, except #BC2-1 for which variations between average values for skeletal growth and equant terminations are shown). Overall, the data for the F-absent composition show $D_{Ba}^{Afs/m.}$ in the range of 18 to 65, and suggest at most a weak dependence on temperature. With 1 wt% added fluorine (Fig. 8b), the effects of zoning and boundary layer gradients are much less pronounced for T≥700 °C, for which $D_{Ba}^{Afs/m.}$ increases demonstrably from ~10 at 700–750 °C up to ~30 at 850 °C. Although crystal zoning also is relatively unimportant for most F-added experiments at T ≤ 650 °C, $D_{Ba}^{Afs/m.}$ follows two distinct trends at low temperature. The trend for short-duration experiments

continues to follow that of decreasing $D_{Ba}^{Afs/m.}$ with decreasing temperature (established at higher T), whereas that for the long-duration experiments bends back toward the higher values observed in the F-absent experiments (and shows more pronounced variation at 550 °C due to crystal zoning).

Discussion

Cesium partitioning and comparison to previous studies

The values of $D_{Ba}^{Afs/m.}$ and $D_{Cs}^{Afs/m.}$ obtained in this study are summarized in Table 3, along with those from a variety of previous studies on both experimental and natural systems. Although the values of $D_{Cs}^{Afs/m.}$ in this study are limited by the detection limit for Cs in feldspar, they are comparable to those of previous studies. Within the uncertainty of the results, the partitioning behavior of Cs did not change as a function of temperature or undercooling.

The effect of Ba on potassium feldspar stability and approach to equilibrium

An important observation from these experiments is that barium extends the stability field of alkali feldspars to higher temperature in granitic liquids. The study of Holtz et al. (1992) indicates that the liquidus temperature for the H_2O-saturated, F- and Ba-absent composition used in this study should be ~760 °C (solidus ~680–690 °C). As liquids in the current experiments were apparently near (or at) H_2O saturation, the liquidus for the Ba- and F-absent composition should fall in the range of ~760–770 °C. From the work of Manning (1981), we would expect a liquidus depression on the order of 40–50 °C with 1 wt% added fluorine, so liquidus temperatures should be in the range of 710–730 °C for the Ba-absent composition with 1 wt% fluorine. In the current experiments, K-dominant, Ba-rich alkali feldspars were produced at temperatures up to 850 °C in the F-absent composition (the rims on celsian), and up to 800–850 °C with 1 wt% added F (and slightly below H_2O saturation). Hence, the data indicate that 0.4–0.5 wt% BaO in the current experimental liquids has extended the liquidus field for Ba-rich alkali feldspar by ~100 °C.

Based on crystal morphology, homogeneity, and steady-state composition over run time, the experiments at T≥800 °C attained, or at least closely approached, bulk equilibrium. Increasingly skeletal crystal morphologies, greater compositional heterogeneity in both crystals and glass, and an absence of quartz in experiments at 650 °C indicate that crystal–melt equilibrium was not maintained during feldspar growth at lower temperatures, and these effects become more pro-

Table 3 Summary of partition coefficients (*n.s.* not specified in reference)

$D_{Ba}^{Afs/melt}$	XOr_{Afs}	$(K/K+N)_{Afs}$	T (°C)	P (MPa)	Reference
Ba partition coefficients ($D_{Ba}^{Afs/melt}$)					
Experimental studies					
15–60	9–79	0.70–0.80	600–850	200	This study: F-absent
3–48	53–89	0.62–0.90	550–850	200	This study: 1 wt% F
6.4–8.7	43–49	0.48–0.54	900–1,000	1,000	Guo and Green (1989)
6.4–14	63–81	75–85	720–780	800	Long (1978)
25–80	40–100	0.40–1.00	700–800	200	Carron and Lagache (1980)
1–19	5–70	0.14–0.82	650–750	200	Icenhower and London (1996)
Studies of natural systems					
0.8–>2.2	5–42	0.06–0.45	n.s.	n.s.	Carmichael and McDonald (1961)
1.17–8.95	36–63	0.39–0.63	n.s.	n.s.	Berlin and Henderson (1969)
0.3–4.8	15–49	0.15–0.51	n.s.	n.s.	Picirillo et al. (1975)
2.7–18.0	n.s.	n.s.	n.s.	n.s.	DePieri and Quareni (1978)
4.9–8	63–65	0.64–0.66	720–790	150–300	Hildreth (1979)
3.4–7.5	45–68	0.48–0.70	775–875	n.s.	Crecraft et al. (1981)
13–44	50–67	0.53–0.69	n.s.	n.s.	Leeman and Phelps (1981)
1.0–6.7	64–66	0.65–0.66	720–850	150–300	Mahood and Hildreth (1983)
0.4–9.8	n.s.	n.s.	n.s.	n.s.	Wörner et al. (1983)
7.2–24.0	45–68	0.48–0.70	775–880	n.s.	Nash and Crecraft (1985)
Cs partition coefficients ($D_{Cs}^{Afs/melt}$)					
Experimental studies					
<0.1	9–89	0.70–0.80	550–850	200	This study: all compositions
<0.1	5–70	0.14–0.82	650–750	200	Icenhower and London (1996)
0.02–0.04	40–100	0.40–1.00	700–800	200	Carron and Lagache (1980)
Studies of natural systems					
0.05–0.07	63–65	0.64–0.66	720–790	150–300	Hildreth (1979)
0.09–0.32	45–68	0.48–0.70	775–875	n.s.	Crecraft et al. (1981)
0.013–0.036	50–55	0.53–0.56	n.s.	n.s.	Leeman and Phelps (1981)
0.009–0.028	41–46	0.41–0.46	850	<200	Mahood (1981)
0.02–0.13	29–63	0.30–0.63	n.s.	n.s.	Drexler et al. (1983)
0.009–0.061	64–66	0.65–0.66	720–850	150–300	Mahood and Hildreth (1983)
0.11–0.16	45–68	0.48–0.70	775–880	n.s.	Nash and Crecraft (1985)

nounced with decreasing run temperature. Note that 800–850 °C experiments at or very near water saturation (i.e., those with 5 wt% added water) produced only about 5 vol% crystals after 14 days. If the true liquidus temperature of the system with ~0.3–0.5 wt% BaO is construed to be ~850 °C, the point at which K-dominant but Ba-rich feldspars were produced, then the bulk of feldspar crystallization in experiments at T ≤ 750 °C occurred in liquids which were undercooled by about 100 °C more than in a Ba-absent analogue composition.

Miscibility of Ba in potassic alkali feldspar

To effectively consider the partitioning behavior of Ba, we must consider whether a solvus exists between Ba-rich and Ba-poor alkali feldspars. The current experiments at low undercooling produced feldspars (discrete zones or entire crystals) containing ~28 to 87% celsian components which are homogeneous by BSEI and/or replicate EMPA using a 2-μm spot (e.g., Fig. 3). These relations suggest continuous solubility of Ba in potassic feldspar over this range of composition. Moreover, the extended stability field for Ba-enriched K-feldspar implies that pure celsian possesses a higher melting temperature than does $KAlSi_3O_8$, and hence the $KAlSi_3O_8$–$BaAl_2Si_2O_8$ melting loop would resemble that of $NaAlSi_3O_8$–$CaAl_2Si_2O_8$. Feldspars with lower celsian contents produced at lower temperatures were strikingly zoned. Although we believe that such zonation is primarily a consequence of growth kinetics (see below), we note that the compositions of individual zones span the gamut of about 2 to 16% celsian. This range is similar to homogeneous cores and relict grains of natural volcanic sanidine having 2–14% celsian components (Webber et al. 1997; Morgan et al. 1998). The sum of the evidence supports complete miscibility between celsian and potassic alkali feldspar at 200 MPa, consistent with the results of previous experimental investigations (Roy 1965, 1967).

Barium partitioning in liquids near equilibrium

Evidence cited above indicates that weakly undercooled (T≥800 °C) experiments with the F-absent composition appear to have approached or attained equilibrium. Values of $D_{Ba}^{Afs/m.}$ average around 18 for the F-absent composition at 800 °C (Fig. 8a), which falls well within the range of values observed in previous studies (Table 3). The consistency of values for all crystals at 800 °C and for K-dominant rims ($Or_{40–60}$) at 850 °C, however, suggests a significant increase in $D_{Ba}^{Afs/m.}$ (from ~18 to ≥40) over this temperature range. A simple dependence of $D_{Ba}^{Afs/m.}$ on temperature over this range is questionable, however, because it may be inappropriate to compare the values for Ba-rich crystals produced at 850 °C with the more K-dominant feldspars from lower temperatures. Rather, the increase in $D_{Ba}^{Afs/m.}$ is likely related to the effect of high barium contents which begin to dominate crystal chemistry above 800 °C (recall the apparent non-Henrian behavior of Ba in Fig. 7a). A crystal-chemical effect appears to be underscored by apparently higher $D_{Ba}^{Afs/m.}$ for extremely celsian-rich cores relative to rims produced at 850 °C, even though the BaO contents of liquid were almost identical.

Temperature-averaged values of $D_{Ba}^{Afs/m.}$ for experiments with 1 wt% added fluorine at T≥750 °C are in the range of 10–25 (Fig. 8b), and are comparable to those of previous studies (Table 3). Textures and homogeneity of crystalline products and glass also support our interpretation that crystal–liquid equilibrium was closely approached, if not fully attained in those experiments. An increase of $D_{Ba}^{Afs/m.}$ with temperature for feldspars produced in the F-added composition at T≥700 °C (Fig. 8b) appears to reflect a true dependence on temperature, as the feldspars produced at 800–850 °C are K-dominant. Deviations in liquidus relations and compositional trends at lower temperatures, however, indicate that the observed $D_{Ba}^{Afs/m.}$ values may not have been produced at conditions close to the bulk crystal–melt equilibrium (discussed further below).

The effects of undercooling in the F-absent system

The principal effects of progressive undercooling on crystalline products are increasingly skeletal to cuneiform crystal morphologies, radial growth habits, and compositional zoning in feldspar. Skeletal morphology and radial growth habit clearly stem from rapid crystal growth, and effectively reproduce the textural result of increasingly skeletal and spherulitic growth morphologies accompanying the equivalence of growth rate and diffusion rate observed by Baker and Freda (2001). Compositional zoning (principally of Ba) in feldspar is not necessarily an artifact of rapid growth, but also could be related to slow lattice diffusion in the solids (Watson and Liang 1995). The variability of $D_{Ba}^{Afs/m.}$ observed in individual experiments at T ≤ 750 °C (Fig. 8a) stems mostly from crystal zoning, but evaluating the utility of effective $D_{Ba}^{Afs/m.}$ values obtained requires further consideration of how Ba contents relate to feldspar growth history and composition.

Although we would expect the consumption of Ba from liquid to cause the BaO contents in feldspar to decline with progressive growth at constant temperature, this was not observed in the bulk sense. As discussed above (Fig. 6), the average BaO contents of feldspars produced at a given temperature were nearly constant between experiments of different duration, regardless of the BaO content of bulk glass. Interestingly, the degree of mineral zoning at a given temperature also was comparable between experiments of 5- and 14-day duration, indicating that if Ba depletion from liquid is responsible for varying Ba contents in crystals, the effect was extremely local. Hence, although the zonal distribution of Ba within crystals may be governed by slow lattice diffusion as envisioned by Watson and Liang (1995), we

suggest that rapid growth stemming from extreme supersaturation is dominantly responsible for producing the spread of feldspar compositions observed in each experiment. The rate of crystal growth is difficult to ascertain from the current experiments, in part because the nucleation lag (time interval before growth of measurable crystals) is unconstrained. Maximum crystal lengths suggest effective growth rates in the range of 6×10^{-9} cm/s to 2×10^{-8} cm/s, but these likely underestimate true growth rates. Maximum crystal lengths are quite similar (vary by less than a factor of 2) between experiments of 5- and 14-day duration at each temperature, suggesting continuous nucleation punctuated by rapid growth. Moreover, crystal growth appears to terminate after a limiting crystal size (75–250 μm, increasing with decreasing temperature) is attained, which may be related to diffusional transport of constituents and/or metastability. The development of boundary layers in liquid which are depleted of crystal-compatible components but enriched in crystal-incompatible components (e.g., Cs) does indicate that crystal growth rates are limited by the rates of component diffusion through liquid. With regard to metastability, we note an apparent absence of low-Ba ($\leq$ 0.4–0.5 wt% BaO) feldspars in all charges. This apparent absence may be due either to vanishingly small abundance stemming from incomplete reaction (due to short run duration) or to complete lack of formation accompanying the loss of the driving force for feldspar crystallization (i.e., a decrease in effective undercooling accompanying the depletion of Ba from liquid).

Icenhower and London (1996) demonstrated a positive correlation between $D_{Ba}^{Afs/m.}$ and Or content of alkali feldspar grown at 200 MPa in the temperature range of 650–750 °C. With this in mind, the partition coefficients determined for all spot analyses of feldspar in F-absent experiments are plotted as a function of molecular K/K + Na in Fig. 9. Considered together, the data for experiments at all temperatures appear to show very poor correlation (Fig. 9a). Examination of the data for experiments at each temperature (Fig. 9b–g), however, shows a high degree of organization defined by a series of linear trends which truncate against the equilibrium line of Icenhower and London (1996). With decreasing temperature, these trends rotate about a pivot point located near $100\times(K/K+N) = 73$–75 and $D_{Ba}^{Afs/m.} \cong 60$, which is equivalent to the average value for the celsian-rich feldspars grown at 850 °C. We deduce that reasonable estimates for the true values of $D_{Ba}^{Afs/m.}$ at lower temperatures should lie near the lower ends of the trends seen in Fig. 9, which are consistent with previous investigations of natural and experimental systems at equilibrium (e.g., near the trend of Icenhower and London 1996). Hence, incipient feldspar growth in these undercooled experiments is marked by transient supersaturation in Ba-rich feldspar having Ba contents up to those produced at high temperature. The net result is that even though growth occurs isothermally at low temperature, the compositions of feldspars grown from the undercoooled liquids record a vestige of the thermal history of the liquids (e.g., Y→Z, Fig. 1). This mirrors observations from some of our previous studies. For example, London et al. (1989) documented early alkali feldspars grown from undercooled Macusani liquids at T ≤ 650 °C to have ternary, hypersolvus compositions which were isothermally succeeded by patchy intergrowth of sodic and potassic pairs at equilibrium on the strain-free alkali feldspar solvus. Akizuki (1983) noted that spherulites produced by the natural devitrification of rhyolitic obsidian at T ≤ 200 °C were disordered, monoclinic sanidine (prior to partial replacement by ordered, triclinic anorthoclase), suggesting that such effects can extend down to temperatures considerably below the glass transition.

The effects of undercooling with 1 wt% added fluorine

With 1 wt% added fluorine and temperatures down to ~700 °C in runs of long duration, and in all short-duration experiments down to 550 °C, crystals and glasses are comparatively homogeneous. Greater homogeneity of crystals and glasses in these experiments (compared to the F-absent system) could result from more rapid elemental diffusion through liquid. Homogeneity, however, also could be explained simply by the lower percentages of crystallization, which causes less depletion of Ba from liquid and may produce boundary layers in liquid too narrow to resolve by EMPA. Values of $D_{Ba}^{Afs/m.}$ in short-duration undercooled experiments decrease with temperature (Figs. 8b, 10b), following the trend noted at higher temperatures but consistently deviating from the equilibrium relation of Icenhower and London (1996). Although the decrease of $D_{Ba}^{Afs/m.}$ with temperature for feldspars produced at T≥700 °C appears to reflect a true dependence on temperature, crystallization lag (metastable persistence of liquid) complicates the correlation with temperature because the $D_{Ba}^{Afs/m.}$ obtained may not represent equilibrium values. This is supported by the two different trends observed in the data from T ≤ 650 °C (Fig. 8b) produced as a function of run duration and, hence, degree of crystallization. Values of $D_{Ba}^{Afs/m.}$ obtained from long-duration experiments below 650 °C become more variable than in short-duration experiments (compare Fig. 10b with Fig. 10c–e), with those at 650 and 550 °C showing heterogeneous behavior like that observed in the F-absent system. These relations indicate a change in apparent partitioning behavior once the lag in crystal nucleation and growth is overcome. Hence, the values of $D_{Ba}^{Afs/m.}$ obtained at all temperatures (and the apparent temperature dependence seen at T≥700 °C) may be affected by similar kinetic lag.

Ramifications for natural magmas and rocks

Ba-rich alkali feldspars in magmatic rocks

The expansion of the liquidus field for K-feldspar due to barium in granitic liquids provides a potential

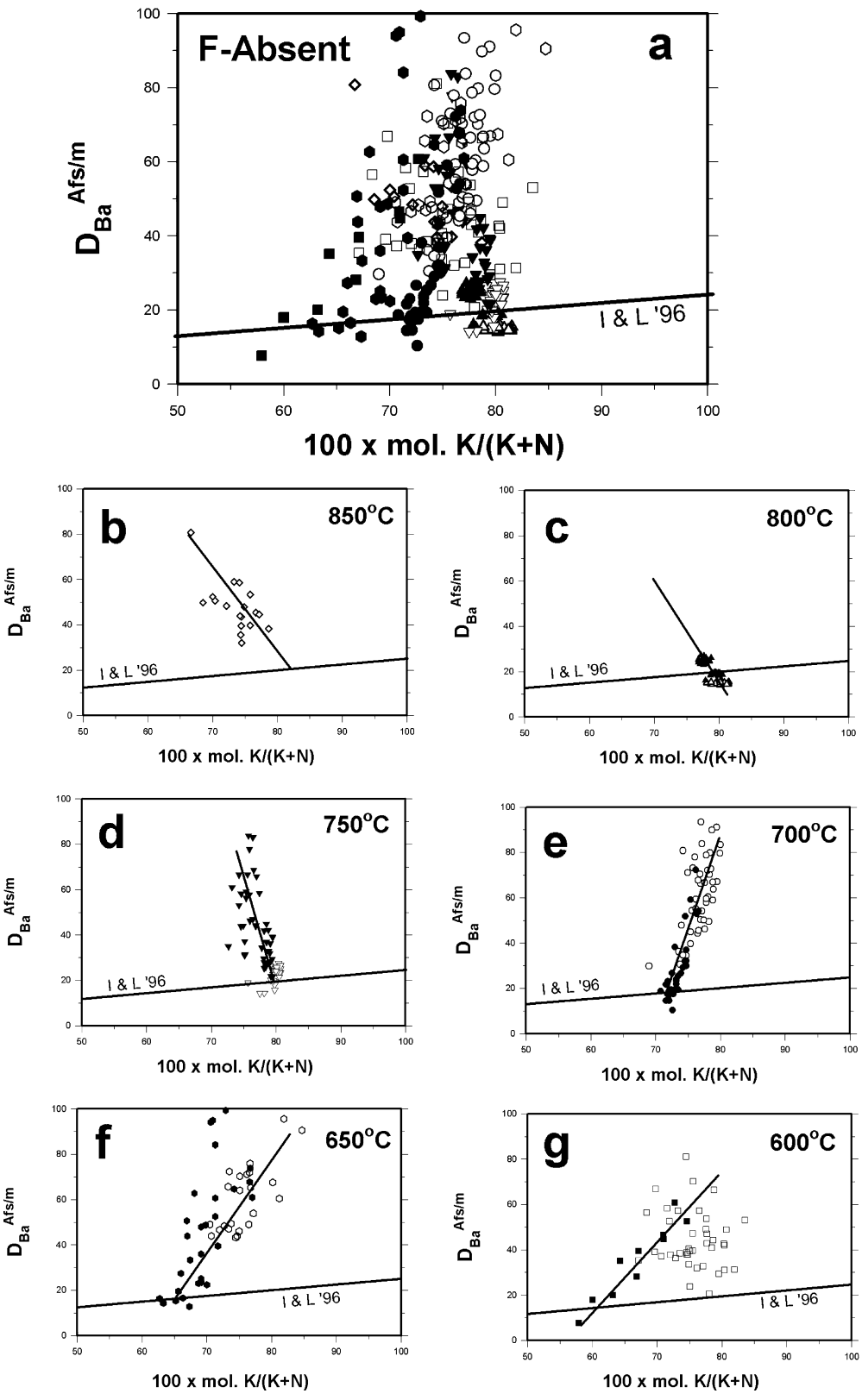

Fig. 9a–g $D_{Ba}^{Afs/m.}$ versus 100×molec. K/K + Na of alkali feldspar for F-absent experiments. *Symbols* in **a** represent different experimental temperatures shown in **b–g**. *Open symbols* are for experiments of 5-day duration; *closed symbols* are for 14-day duration. *Solid line* labeled *I & L '96* is the equilibrium trend of Icenhower and London (1996). Other *solid lines* represent inferred trends (see text)

explanation for anomalously barian K-feldspars in some natural settings. Two such examples include peraluminous volcanic rocks, from the Los Indios tuff of Central Mexico (Webber et al. 1997) and quartz latites of the Morococala field, Bolivia (Morgan et al. 1998). In these rocks, Ba-rich potassic alkali feldspar (Los Indios up to 14 mol% celsian; Morococala up to 3–4 mol% celsian) is preserved as anhedral and embayed (resorbed) crystal

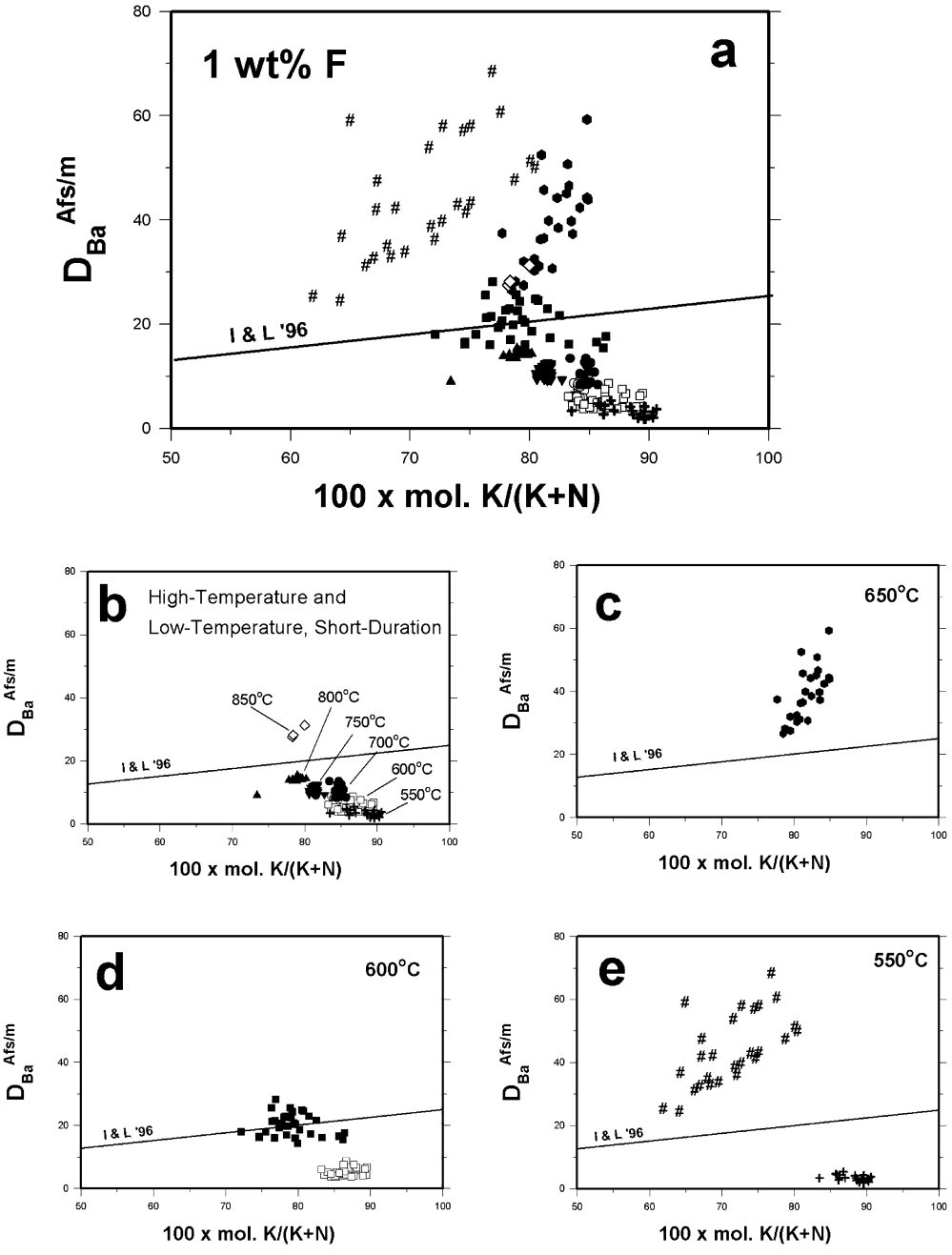

Fig. 10a–e $D_{Ba}^{Afs/m.}$ versus 100×molec. K/K + Na of alkali feldspar for F-bearing experiments. *Symbols* are the same as in Fig. 8, except for experiments at 550 °C for which + denotes 5-day duration, and # 14-day duration. *Solid line* labeled *I & L '96* is the equilibrium trend of Icenhower and London (1996)

fragments and/or resorbed cores overgrown by sanidine rims with much lower BaO contents. In both cases, the Ba-rich feldspars were interpreted as xenocrystic crystal fragments. We feel that they likely represent restitic crystals which were enriched in Ba during anatexis. The substantial increase of $D_{Ba}^{Afs/m.}$ noted in current experiments near equilibrium, along with sanidine cores having BaO contents an order of magnitude higher than the rims in the natural rocks (Webber et al. 1997; Morgan et al. 1998), suggest that small quantities of very barium-rich alkali feldspar can be produced as restite in comparatively Ba-poor systems. For example, Morgan et al. (1998) noted < 1 vol% Ba-rich sanidine fragments and cores in the Morococala quartz latite which were interpreted to have been generated at T > 750 °C. A whole-rock Ba content of 905 ppm in the latite coupled with $D_{Ba}^{Afs/m.}$ ~20 at 800 °C from the current experiments is quite consistent with generation of the most Ba-rich sanidine crystals having 1.4–1.8 wt% elemental Ba. The current experiments at 850 °C yield observed values of $D_{Ba}^{Afs/m.}$ in the range of 40–80. Hence, feldspars produced at higher temperatures (e.g., during anatexis at ≥850 °C) from a liquid comparable to the Morococala quartz latite (905 ppm Ba) should be richer in Ba (up to 7.2 wt% in the crystals), but feldspar compositions comparable to those in the Morococala quartz latite could be produced from liquids containing only 175–450 ppm Ba.

Feldspar compositions as indicators of fractionation in undercooled systems

The large differences observed in average $D_{Ba}^{Afs/m.}$ between short- and long-duration experiments at $T \leq 700$ °C, especially for the F-added composition, are due almost exclusively to differences in BaO contents of glass. As was discussed above (e.g., Fig. 6a), the average BaO contents of feldspar at a given temperature are surprisingly consistent and high in undercooled experiments containing less than about 30–35% crystals. It remains unclear, however, if the high BaO contents (high apparent $D_{Ba}^{Afs/m.}$) produced during incipient feldspar growth via supersaturation observed in the current experiments would be a transient phenomenon in nature. Clearly, if growth were to continue in the current, small-volume experiments, high-Ba feldspars produced by initial supersaturation must be succeeded by the growth of Ba-poorer feldspar accompanying the depletion of Ba from liquid, perhaps coupled with an approach to equilibrium behavior as undercooled liquids overcome lags in nucleation and growth. The net result would be the development of normal zonation with respect to compatible trace elements during isothermal growth which is similar to, but likely more extreme (e.g., Y→Z, Fig. 1) and discontinuous than, that which would be produced by fractionation accompanying decreasing temperature in systems at equilibrium. Compounding the effect of supersaturation on initial crystal growth in undercooled liquids, however, are the production of boundary layers in liquid, and the larger scale and temperature gradients endemic to the natural systems. Incipient growth accompanying supersaturation will cause the depletion of compatible components from the boundary layers around crystals, and thus continued growth would occur from liquids markedly different from the bulk liquid composition. Crystallization through a boundary layer, especially a laterally continuous one sweeping through a large undercooled body, could conceivably result in no significant change in the concentration of trace elements following the initial period of growth which produced the boundary layer. The concentrations of such trace elements, however, would not be reflective of the equilibrium $K_d(i)^{Xtal/liq}$. In this regard, tourmaline systematics in the Little Three Pegmatite, California seem instructive (Morgan and London 1999). In the footwall aplite of that body, tourmaline shows an inward change in morphology, from anhedral and interstitial in the weakly lineated, outer portion to euhedral in the strongly lineated (and volumetrically larger), interior "line rock". This change in morphology records a respective change from late (anhedral) to early (euhedral) tourmaline growth in the crystallization sequence, and Morgan and London (1999) suggested that the formation of euhedral tourmaline in the "line rock" marked the point at which a laterally continuous boundary layer was produced which was sufficiently enriched in boron (2–3 wt% B_2O_3 in similar compositions; Wolf and London 1997) to cause saturation in tourmaline as an early liquidus phase (note that B_2O_3 in the whole-rock composition is below tourmaline saturation). Even though F is compatible ($D_F^{Tur/liq} = 3$; Wolf and London 1997) in the schorl–olenite–foitite tourmaline ("SOFTur") solid solutions which occur throughout most of the body (everywhere except at, or within, central pocket zones which contain F-rich elbaitic tourmaline), the F contents of SOFTur remain constant and low, rather than increasing as would be predicted from either Rayleigh fractionation or zone refining models. Hence, tourmaline compositions throughout most of the crystallization of the Little Three body appear to reflect the near steady-state composition of a boundary layer rather than the bulk composition of the body, even as modified by progressive crystal fractionation. In total, then, the effects of supersaturation and growth involving boundary layers lend considerable uncertainty to using the concentrations of compatible trace elements for modeling fractionation in undercooled liquids.

An area of curiosity going in to this study was whether supersaturation would notably increase the partition coefficient for an incompatible (or mildly compatible) component, particularly if crystal growth rates approach the rates of diffusion for such components. For example, Lindstrom et al. (1979) noted a four-fold increase in the olivine/liquid partition coefficient for Sm (0.0038 to 0.016) accompanying an increase in cooling rate from 30 to 410 °C per hour, and indicated the result was expected based on the increase in olivine growth rate. Conversely, Baker and Freda (2001) noted no change in partitioning behavior for mildly compatible Rb between alkali feldspar and liquid ($D_{Rb}^{Kfs/liq} \sim 1$) on undercooling from 50 to 200 °C, even though the experimental products show a change in habit from euhedral single crystals to radial-skeletal growth. Although Cs-enriched boundary layers were produced around crystal clusters in the current undercooled experiments, no detectable change of $D_{Cs}^{Afs/m.}$ was found. We observed no changes in product textures (e.g., London and Morgan 1998) indicating that any experiment crossed a glass transition. Hence, we have no direct evidence for behavior below the glass transition, at which point elemental diffusivities should show a pronounced decrease. The current experiments, however, indicate that, at least in supercooled liquids, incompatible components like Cs will be progressively enriched in boundary layer liquids until their concentration causes local saturation in an accessory phase (e.g., pollucite or Cs-analcime: London 1986; London et al. 1998).

Crystallization in the current experiments either ceased (by virtue of metastable persistence of melt) or was halted (by quenching), and thus little (if any) sodic feldspar was produced. Consequently, these experiments shed no light on the effect of undercooling on major-element systematics. We have noted from previous experiments (London et al. 1989; London and Morgan 1998) and studies of natural systems (e.g., Morgan and London 1999) that alkali feldspars produced in undercooled systems eventually evolve to growth of potassic and sodic pairs appropriate to the strain-free

solvus at the temperature of growth. This suggests little effect of undercooling on the major-element (Na–K) systematics of the alkali feldspars. Such studies, however, utilized systems with trace-level Ba contents, and thus we cannot speculate about the effects of additional, highly compatible components on major-element systematics in systems either near the liquidus or far from equilibrium. For example, several previous studies have shown that Ba is much more compatible in potassic feldspar than in sodic feldspar. From the current results, it is uncertain as to whether the addition of Ba may enhance immiscibility between potassic and sodic feldspars such that the solvus between alkali feldspar and plagioclase is expanded.

Conclusions

The current experiments allow us to draw several general conclusions concerning the effect of Ba and minor/trace-element partitioning between alkali feldspar and silicic liquid.

1. Barium extends the stability field of potassic alkali feldspar to higher temperatures, and $D_{Ba}^{Afs/m.}$ increases both with temperature and as Ba in feldspar increases to become the dominant component at high temperature. This behavior suggests that anomalously barian alkali feldspars may be a natural consequence of high-temperature reaction, especially being produced in restite during crustal anatexis.
2. Barium apparently shows continuous solubility in potassic alkali feldspar, such that there is complete miscibility between Or and Cel components.
3. In the range of undercooling examined, supersaturation accompanying undercooling causes increased incorporation of compatible components (incipient growth with apparent average $D_{Ba}^{Afs/m.}$ well above equilibrium behavior) but has little effect on the behavior of strongly incompatible components ($D_{Cs}^{Afs/m.}$ showed no resolvable effect). Even though growth occurs isothermally at low temperature, early feldspar crystals in rapidly undercooled liquids are marked by concentrations of highly compatible components, especially those for which $D_i^{Afs/m.}$ increase with temperature, more appropriate to the precooled state (i.e., temperature of intrusion) than to the actual temperature of growth.
4. Increasing fluorine contents exacerbate the effects of undercooling on fractionation of silicic liquids near water saturation by inhibiting feldspar nucleation, such that both the partitioning behavior and K/K + Na for incipient growth deviate from equilibrium. Significant growth and approach to equilibrium partitioning behavior of alkali feldspar are delayed in time and temperature until the lag in nucleation is overcome, producing a period of rapid growth from supersaturated liquid similar to F-absent compositions.
5. Changes in effective partition coefficients for alkali feldspar away from equilibrium relations accompanying supersaturation, coupled with the production of boundary layers in liquid, lend considerable uncertainty to the use of highly compatible trace elements for modeling fractionation in undercooled silicic magmas. Barring subsolidus annealing, however, the compositional variability produced may record the temperature history of an undercooled body within individual, zoned feldspar crystals.

Acknowledgments Funding for this work was provided by National Science Foundation grant EAR-990165. The Electron Microprobe Laboratory at the University of Oklahoma was created by Department of Energy Grant DE-FG22-87FE1146 and National Science Foundation EAR-8720498, with annual operational support from the Office of the Vice Provost of Research. We thank Alberto Patiño-Douce and an anonymous reviewer for their constructive remarks.

References

Akizuki M (1983) An electron microscopic study of anorthoclase spherulites. Lithos 16: 249–254

Baker DR, Freda C (2001) Eutectic crystallization in the undercooled orthoclase-quartz-H_2O system: experiments and simulations. Eur J Mineral 13:453–466

Berlin R, Henderson CMB (1969) The distribution of Sr and Ba between alkali feldspar, plagioclase and groundmass phases of porphyritic trachytes and phonolites. Geochim Cosmochim Acta 33:247–255

Blundy J, Wood B (1994) Prediction of crystal-melt partition coefficients from elastic moduli. Nature 372:452–454

Carmichael I, McDonald A (1961) The geochemistry of some natural acid glasses form the North Atlantic Tertiary volcanic province. Geochim Cosmochim Acta 25:189–222

Carron JP, Lagache M. (1980) Étude expérimentale du fractionnement des éléments Rb, Cs, Sr, et Ba entre feldspaths alcalins, solutions hydrothermales, et liquides silicatés dans le système Q.An.Or.H2O à 2 kbar entre 700 et 800°C. Bull Mineral 103:571–578

Christiensen EH, Bikun JV, Sheridan MF, Burt DM (1984) Geochemical evolution of topaz rhyolites from the Thomas Range and Spoor Mountain, Utah. Am Mineral 69:223–236

Crecraft HR, Nash WP, Evans SH Jr (1981) Late Cenozoic volcanism at Twin Peaks, Utah: geology and petrology. J Geophys Res 86:10303–10320

De Pieri R, Quareni S (1978) Partition coefficients of alkali and alkaline-earth elements between alkali feldspar phenocrysts and their lava matrix. Mineral Mag 42:63–67

Dingwell DB, Scarfe SM, Cronin D (1985) The effect of fluorine on viscosities in the system Na_2O-Al_2O_3-SiO_2: implications for phonolites, trachytes, and rhyolites. Am Mineral 70:80–87

Drexler JW, Bornhorst TJ, Noble DC (1983) Trace-element sanidine/glass distribution coefficients for peralkaline silicic rocks and their implications to peralkaline petrogenesis. Lithos 16:265–271

Fenn PM (1977) The nucleation and growth of alkali feldspars from hydrous melts. Can Mineral 15:135–161

Guo J, Green TH (1989) Barium partitioning between alkali feldspar and silicate liquid at high temperature and pressure. Contrib Mineral Petrol 102:328–335

Hamilton DL, Henderson CMB (1968) The preparation of silicate compositions by a gelling technique. Mineral Mag 36:832–836

Harris NBW, Inger S (1992) Trace element modelling of pelite-derived granites. Contrib Mineral Petrol 110:46–56

Hildreth W (1979) The Bishop Tuff: evidence for the origin of compositional zonation in silicic magma chambers. Geol Soc Am Spec Pap 180:43–75

Holtz F, Pichavant M, Barbey P, Johannes W (1992) The effect of H_2O on liquidus phase relations in the haplogranite system at 2 and 5 kbar. Am Mineral 77:1223–1241

Icenhower J, London D (1996) Experimental partitioning of Rb, Cs, Sr, and Ba between alkali feldspar and peraluminous melt. Am Mineral 81:719–734

Irving AJ (1978) A review of experimental studies of crystal/liquid trace element partitioning. Geochim Cosmochim Acta 42:743–770

Kovalenko VI, Kovalenko NI (1984) Problems of the origin, ore-bearing, and evolution of rare-metal granitoids. Phys Earth Planet Interiors 35:51–62

Leeman WP, Phelps DW (1981) Partitioning of rare earths and other trace elements between sanidine and coexisting volcanic glass. J Geophys Res 86:10193–10199

Lindstrom DJ, Lofgren GE, Haskin LA (1979) Experimental studies of kinetic effects on trace element partitioning. Abstr EOS 60:402

London D (1986) The magmatic-hydrothermal transition in the Tanco rare-element pegmatite: evidence from fluid inclusions and phase equilibrium experiments. Am Mineral 71:376–395

London D (1987) Internal differentiation of rare-element pegmatites: effects of boron, phosphorus, and fluorine. Geochim Cosmochim Acta 51:403–420

London D (1992) The application of experimental petrology to the genesis and crystallization of granitic pegmatites. Can Mineral 30:499–540

London D, Morgan GB VI (1998) Experimental crystal growth from undercooled granitic melts: nucleation response, texture, and crystallization sequence. Am Geophys Union Abstr Program 79:5366

London D, Morgan GB VI, Hervig RL (1989) Vapor-undersaturated experiments with Macusani glass + H_2O at 200 MPa, and the internal differentiation of granitic pegmatites. Contrib Mineral Petrol 102:1–17

London D, Morgan GB VI, Icenhower J (1998) Stability and solubility of pollucite in granitic systems at 200 MPa H_2O. Can Mineral 36:497–510

London D, Morgan GB VI, Wolf MB (2001) Amblygonite-montebrasite solid solutions as monitors of fluorine in evolved granitic and pegmatic melts. Am Mineral 86:225–233

Long PE (1978) Experimental determination of partition coefficients for Rb, Sr, and Ba between alkali feldspar and silicate liquid. Geochim Cosmochim Acta 42:833–846

Mahood GA (1981) Chemical evolution of a late Pleistocene rhyolitic center: Sierra La Primavera, Jalisco, Mexico. Contrib Mineral Petrol 77:129–149

Mahood G, Hildreth W (1983) Large partition coefficients for trace elements in high-silica rhyolites. Geochim Cosmochim Acta 47:11–30

Manning DAC (1981) The effect of fluorine on liquidus phase relationships in the system Qz-Ab-Or with excess water at 1 kbar. Contrib Mineral Petrol 76:206–215

McCarthy TS, Hasty RA (1976) Trace element distribution patterns and their relationship to the crystallization of granitic melts. Geochim Cosmochim Acta 40:1351–1358

Morgan GB VI, London D (1996) Optimizing the electron microprobe analysis of hydrous alkali aluminosilicate glasses. Am Mineral 81:1176–1185

Morgan GB VI, London D (1999) Crystallization of the Little Three layered pegmatite-aplite dike, Ramona District, California. Contrib Mineral Petrol 136:310–330

Morgan GB VI, London D, Luedke RG (1998) Petrochemistry of peraluminous silicic volcanic rocks from the Morococala field, Bolivia. J Petrol 39:601–632

Nash WP, Crecraft HR (1985) Partition coefficients for trace elements in silicic magmas. Geochim Cosmochim Acta 49:2309–2322

Picirillo EM, Gregnanin A, De Pieri R (1975) Le ignimbriti della formazione oliocenia di Alagi (Altopiano Etiopico Centrale). Atti Mem Accad Paavina Sci Pett Art 87(II) Sci Mat Nat:51–90

Pouchou JL, Pichoir F (1985) "PAP" $\phi(\rho z)$ correction procedure for improved quantitative microanalysis. In: Armstrong JT (ed) Microbeam analysis. San Francisco Press, San Francisco, pp 104–106

Roy NN (1965) The binary system: $KAlSi_3O_8$-$BaAl_2Si_2O_8$. Nature 206:501–502

Roy NN (1967) The mineralogy of the potassium-barium feldspar series. II. Studies on hydrothermally synthesized members. Mineral Mag 36:43–49

Silver L, Stolper E (1989) Water in albitic glasses. J Petrol 30:667–709

Swanson SE, Fenn PM (1992) The effect of F and Cl on the kinetics of albite crystallization; a model for granitic pegmatites? Can Mineral 30:549–559

Tilley RJD (1987) Defect crystal chemistry. Blackie, London

Tuttle OF, Bowen NL (1958) Origin of granite in the light of experimental studies in the system $NaAlSi_3O_8$-$KAlSi_3O_8$-SiO_2-H_2O. Geol Soc Am Mem 74

Watson EB, Liang Y (1995) A simple model for sector zoning in slowly grown crystals: Implications for growth rate and lattice diffusion, with emphasis on accessory minerals in crustal rocks. Am Mineral 80:1179–1187

Webber KL, Falster AU, Simmons WB (1997) Zoned, barium-enriched alkali feldspars from Juchipila, Zacatecas, Mexico: evidence for lower-crustal xenocrysts. Rocks Miner 72:190–191

Webber KL, Simmons WB, Falster AU (1999) Cooling rates and crystallization dynamics of shallow level pegmatite-aplite dikes, San Diego County, California. Am Mineral 84:708–717

Wolf MB, London D (1997) Boron in granitic magmas: stability of tourmaline in equilibrium with biotite and cordierite. Contrib Mineral Petrol 130:12–30

Wörner G, Beusen J-M, Duchateau N, Gijbels R, Schmincke H-U (1983) Trace element abundances and mineral/melt distribution coefficients in phonolites from the Laacher See Volcano (Germany). Contrib Mineral Petrol 84:152–173

Wyllie PJ, Tuttle OF (1961) Experimental investigation of silicate systems containing two volatile components. II. The effects of NH_3 and HF, in addition to H_2O, on the melting temperatures of albite and granite. Am J Sci 259:128–143